Measurements of Small-Scale Fading and Path Loss for Long Range RF Tags

Daeyoung Kim, *Member, IEEE*, Mary Ann Ingram, *Member, IEEE*, and W. Whit Smith, Jr., *Member, IEEE*

***Abstract*—RF modulated backscatter (RFMB), also known as modulated radar cross section or sigma modulation, is a RF transmission technique useful for short-range, low-data-rate applications, such as nonstop toll collection, electronic shelf tags, freight container identification and chassis identification in automobile manufacturing, that are constrained to have extremely low power requirements. The small-scale fading observed on the backscattered signal has deeper fades than the signal from a traditional one-way link of the same range in the same environment because the fading on the backscattered signal is the product of the fading on the off-board-generated carrier times the fading on the reflected signal. This paper considers the continuous wave (CW) type of RFMB, in which the interrogator transmitter and receiver antennas are different. This two-way link also doubles the path loss exponent of the one-way link. This paper presents the cumulative distribution functions for the measured small-scale fading and the measured path loss for short ranges in an indoor environment at 2.4 GHz over this type of link.**

***Index Terms*—Electronic shelf tag, modulated backscatter, multipath fading, path loss, reflection antennas, RF tag.**

I. Introduction

LONG range RF tags or RF transponders have various applications, which include nonstop toll collection [1], electronic shelf tags (ESTs) [2], freight container identification and chassis identification in automobile manufacturing [3]. The tags use modulated backscatter, also known as modulated radar cross section or sigma modulation, to transmit information from the RF tag to the interrogator [3]. Their range is typically short, 1–15 m, and their data rates are low, up to tens of kbps [3]–[5]. Because they have no power amplifier, their batteries can last as long as 10 years [3].

Modulated backscatter operation is illustrated in Fig. 1. The low-power transmitter is indicated as the "reflection antenna" in the figure. The RF carrier is generated off-board at Antenna 1. The terminals of the reflection antenna are switched alternately between open and closed states, according to the switch control function, thereby convey information by modulating the reflected signal [2], [3]. The backscattered signal is received by Antenna 2. There is also an unmodulated signal propagating between Antenna 1 and Antenna 2. Since this signal has no information and may cause saturation of receiver components, Antennas 1 and 2 should be appropriately separated, and the receiver at Antenna 2 must filter out the carrier component.

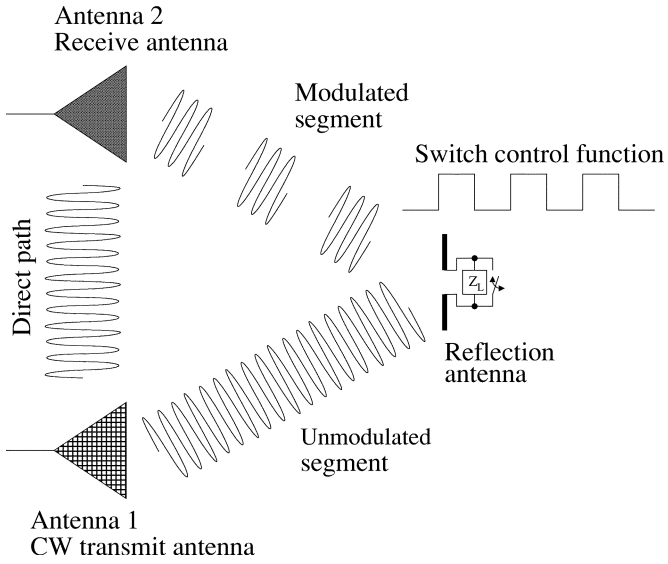

Fig. 1. Modulated backscattered signals.

There are two segments of propagation for this type of link: antenna 1-to-reflection antenna (unmodulated segment) and reflection antenna-to-Antenna 2 (modulated segment). The two-way nature of this link means that the path loss for a symmetric geometry follows $1/d^4$ in free space, where d is distance of one segment [3], [6]. The path loss is described in detail in Section IV. The small-scale fading observed on the backscattered signal has deeper fades than a signal received over a traditional one-way link of the same range in the same environment. This happens because the fading on the backscattered signal is a product of the fades on the two segments.

This paper presents the measured cumulative distribution functions (cdfs) for the small-scale fading and the median path loss at 2.4 GHz over this type of link. One goal of this paper is to determine the theoretical distributions that best fit the measured data in different environments. Others are to verify that the small-scale fading for the modulated backscatter channel can be modeled by the product of two uncorrelated one-way fades and path loss exponent of the two-way link is double that of the one-way link. We first explain the measurement setup and procedure. Next the measured cdfs are compared with some theoretical cdfs using mean square error (MSE)-based goodness-of-fit tests, and finally the median path loss exponent is determined.

Manuscript received February 26, 2002; revised July 22, 2002. This paper appears in part the Proceedings of the Fall Vehicular Technology Conference (VTC) 2001, vol. 3, pp. 1616–1620.

D. Kim was with the School of Electrical and Computer Engineering, Georgia Institute of Technology, Atlanta, GA 30332-0250 USA. He is now with Samsung Electronics Company Ltd., Suwon, Gyeonggi 442-742, Korea (e-mail: daey.kim@samsung.com).

M. A. Ingram and W. W. Smith, Jr. are with the School of Electrical and Computer Engineering, Georgia Institute of Technology, Atlanta, GA 30332-0250 USA (e-mail: maryann.ingram@ece.gatech.edu; whit.smith@ece.gatech.edu).

Digital Object Identifier 10.1109/TAP.2003.814752

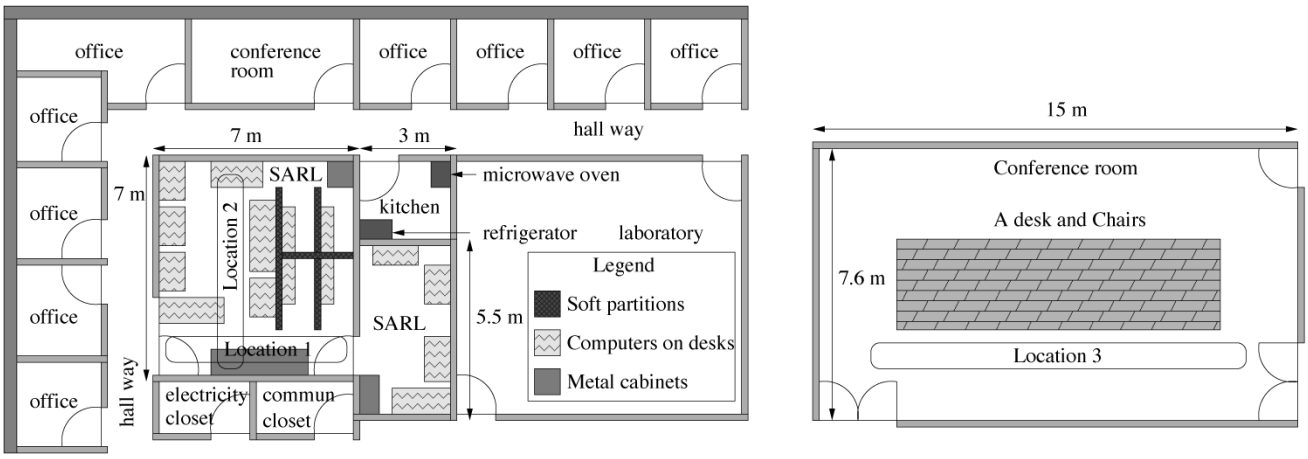

Fig. 2. Partial floor plan of the fifth floor of the GCATT building.

II. Measurement Setup and Procedures

Most of the measurements were taken in the Smart Antenna Research Laboratory at Georgia Tech, a usual small office environment with soft partitions, desks, computers, metal cabinets, and bookshelves. The laboratory is located on the fifth floor of the five-story Georgia Centers for Advanced Telecommunications Technology (GCATT) building. Some other measurements were taken in a lightly cluttered conference room on the same floor but about 10 m away from the laboratory. A couple of chairs around a big table are in the conference room. A partial floor plan of the fifth floor is shown in Fig. 2. Note that there is a kitchen next to the laboratory. The microwave oven in there was disabled during the measurements because its operating frequency (2.45 GHz) is in our measurement frequency band (2.4–2.4835 GHz). The measurements were taken at night and on the weekend to minimize movement in the environment.

A. The Measurement Setup

The measurement setup is shown in Fig. 3. For our reflection antenna, we used the nearly omnidirectional antenna on the EST from the DecisioNet system [2]. The EST was modified to allow the antenna to be switched continuously by an HP33120A function generator at a rate of 25 kHz with a 50% duty cycle. The EST was attached to the side of the T-shaped fixture made of plastic, as shown in Fig. 4. The unmodulated RF carrier was transmitted by a patch antenna, which was hung just below the suspended ceiling and pointed to the EST, indicated by Antenna 1 in Fig. 3. The backscattered signal was received by an active patch antenna, also hung just below the ceiling and pointed to the EST, indicated by Antenna 2 in Fig. 3. Both patch antennas had right-hand circular polarization and a peak gain of 4 dBi. The antenna patterns are omnidirectional in azimuth and hemispherical in elevation, as shown in Fig. 5, in which the contour scale is 5 dB per division [7].

The active antenna included the low-noise amplifier (LNA) HP INA-10386. Its output signal went to a modification of the DecisioNet ceiling base station (CBS), which included amplifiers, a mixer, and an eighth-order filter and which produced I and Q outputs. The local oscillator (LO) for the mixer was detuned by 1 kHz, which is a method to avoid signal cancellation [8] and to get IF conversion, and the I output at 26 kHz was monitored on an audio spectrum analyzer. A computer controlled all instruments through GPIB and RS-232C interfaces and collected data for analysis.

B. The Measurement Procedure for Small-Scale Fading

To measure small-scale fading, the EST was moved in a localized volume using X, Y, and Z actuators on a cart, which is shown in Fig. 4. The scanning distance on the X actuator was 50 cm, which equals four wavelengths (4 λ) at 2.4 GHz, and 400 samples were taken uniformly over its length. Therefore, the sampling interval was 0.125 cm, and this gave enough resolution not to miss the deepest fades. The X axis scans were repeated at five Y axis positions with 10 cm separations and at two Z axis positions with 5 cm separation. Since half-wavelength separation is usually considered sufficient in indoor environments to achieve uncorrelated fading [9], we assume the Y separation of 0.8 wavelength yields uncorrelated fading. Although we do not have data or references to indicate coherence distance in the Z direction, we note that the difference in heights between the ceiling antennas and the tag antenna will provide a significant elevation angular spread in the multipath. Thus, a total of 4000 samples was taken across the volume.

To increase the sample size and thereby improve the quality of our cdf estimates, the volume scan was repeated at 2.4, 2.44, and 2.48 GHz. The 40 MHz separation gives uncorrelated data in indoor channels [10]. Therefore, by combining volume scanning with frequency stepping, we were able to generate 12 000 samples. The data within each frequency set was normalized by its average value before combining the frequency sets to remove the effects of different system responses at these frequencies.

Since two samples separated by 0.5 λ are considered uncorrelated [9], [11], there are approximately 10 uncorrelated samples on the X axis. Therefore, the set of 12 000 samples comprises 40 subsets such that each subset contains 300 uncorrelated samples. This compromise between correlated and uncorrelated samples was necessary to not miss sampling the narrow, deep nulls. According to the Kolmogorov-Smirnov two-sided test, the measured distribution for the uncorrelated samples is within $\pm 7\%$ of the true distributions with a confidence level of 90% [12], [13].

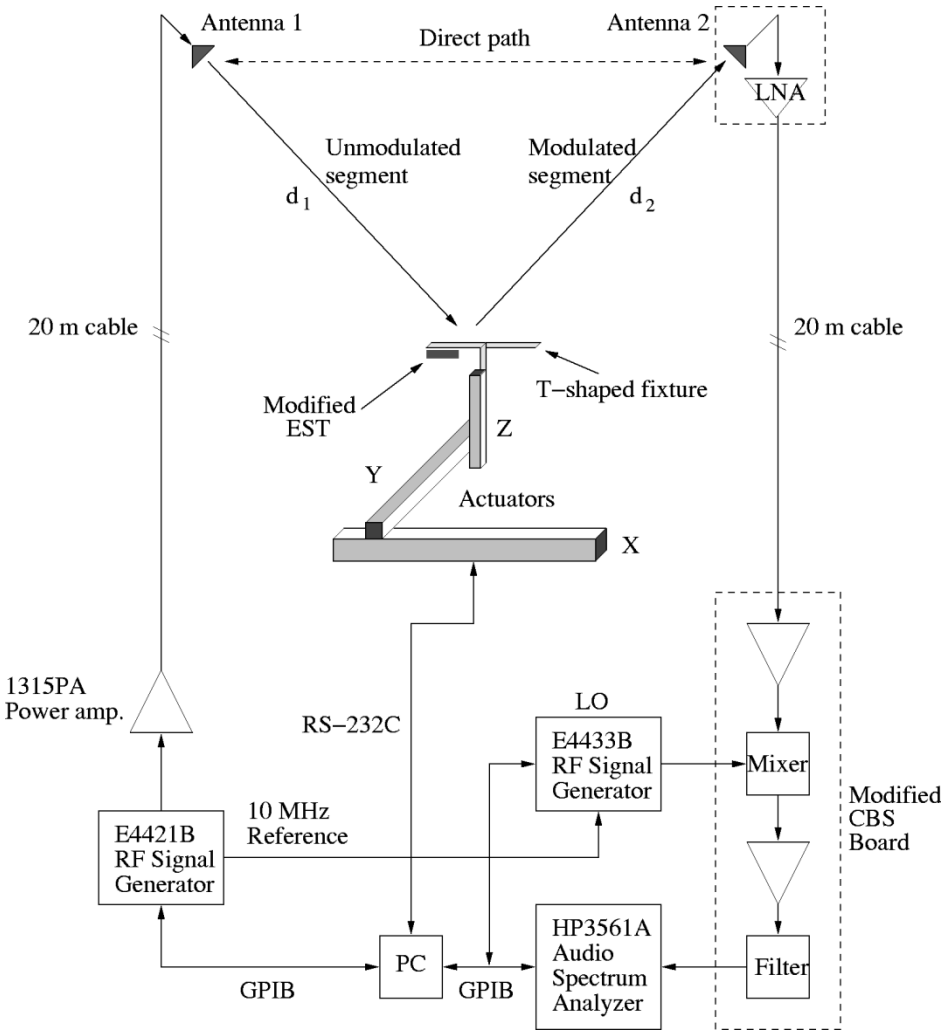

Fig. 3. Measurement setup for two-way propagation.

The data were collected at Locations 1, 2, and 3 in Fig. 2 with the symmetric geometry shown in Fig. 3. For these measurements, Antennas 1 and 2 were attached to the ceiling and pointed to the EST, and the EST was placed half way between Antennas 1 and 2. The three antennas were in a plane that was perpendicular to the ceiling. The lengths of the segments, d_1 and d_2, were both 4 m for Locations 1 and 2; for Location 3, the lengths were 7 m. The distance between Antennas 1 and 2 was 7 m for Locations 1 and 2; for Location 3, the distance was 15 m. The floor-to-ceiling heights were 2.7 m for Locations 1 and 2 and 3.2 m for Location 3.

For Locations 1 and 3, the fades along individual segments and the two-way fades were measured in order to confirm that the two-way fade is the product of two one-way fades. For each location, the one-way and two-way measurements were made consecutively. In the measurement setup for the one-way measurement, the active antenna at Antenna 2 was replaced with a passive one similar to Antenna 1 and both passive Antennas 1 and 2 were used for transmission. Two RF signal generators, which were directly connected to the two antennas, transmitted CW alternately in time. The modified EST in Fig. 3 was again modified to receive the faded signal continuously, and the peak amplitudes at the RF frequency were captured by the RF spectrum analyzer.

C. The Measurement Procedure for Median Path Loss

The median path loss was measured on the contours that have same geometric mean $(\sqrt{d_1 d_2})$ of the distance of the unmodulated and the modulated segments, i.e., d_1 and d_2, in the conference room shown in Fig. 2. Three sets of contours with different antenna separations of Antennas 1 and 2 were considered for this measurement. These contours are shown in Figs. 13–15 and explained in detail in Section IV.

The Antennas 1 and 2 shown in Fig. 3 were attached to the ceiling but pointed to the floor in contrast to the small-scale fading measurements, for which the both antennas were pointed to the EST. Antennas 1 and 2 have directional patterns in elevation, which means that as the EST is moved along the contour, the changing antenna gains with respect to elevation must be appropriately compensated for in the path loss measurements.

To get a local median value, 110 uncorrelated samples were collected in a local volume, $50 \times 40 \times 5$ cm^3. In contrast to the small-scale fading, only 11 samples separated by 5 cm on the *X* axis were taken for a local median value.

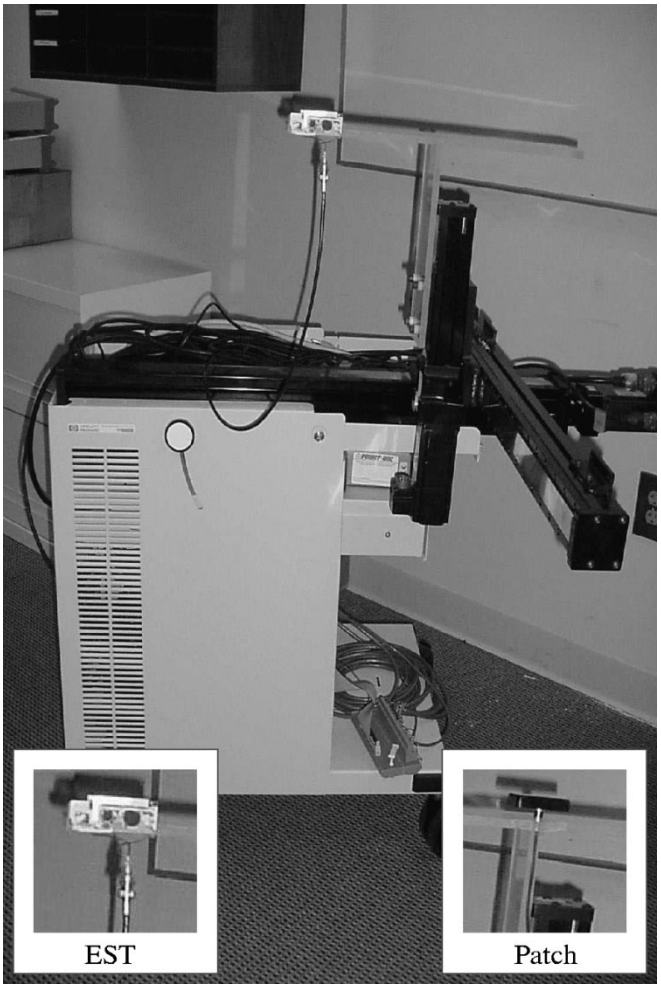

Fig. 4. EST and patch setup on *X*, *Y*, and *Z* actuators on a cart.

III. Analysis of the Measured Small-Scale Fading

A. Comparisons of One-Way Measurements With Different Antennas

To better understand the two-way channel, we performed one-way measurements in the same location, keeping the same relative distances between the antennas the same as in the two-way measurements. To see the effect of a different reflection antenna (i.e., tag), we repeated the one-way measurements using the patch antenna in place of the EST. Fig. 6 shows the cdfs of the one-way fades with the EST antenna for Location 3. Fig. 7 shows the cdfs of the one-way measurement with the patch antenna serving as the reflection antenna, again for Location 3. In these figures, '*' and 'o' correspond to the fading cdfs for the unmodulated and modulated segments with two different antennas, respectively.

By the data-fitting method to be described in Section III-C, the Rician K factors with the patch antenna were always higher than with the EST antenna. Specifically the K factor differences for the segment fades were 2.9 dB and 7.1 dB, respectively. Though not shown on the graph, the differences in K factors were 0.2 dB and 7.7 dB, respectively, for Location 1 and 5.7 dB and 1.7 dB, respectively, for Location 2. Since a higher K factor is normally associated with a stronger LOS, we conclude that the patch antenna has more gain in the LOS directions than the EST antenna in this measurement geometry.

B. The Envelopes of the Faded Signal

Fig. 8 shows the measured data using the EST for five scans along the *X* actuator for one *Z* position and five *Y* positions, respectively. This faded signal was collected for Location 1. The horizontal axis indicates the position of the EST on the *X* actuator and the vertical axis indicates the strength of the first harmonic of the backscattered signal in dBm. The difference between the maximum and minimum signal levels is observed to be 55 dB for this system configuration.[1] The deep nulls in some of the scans may be explained by strong reflections from metal bookshelves near the EST.

C. The Measured cdfs

The cdfs of the measured data for the three locations are compared with three theoretical cdfs: "XYRician", Nakagami, and log-normal. "XYRician" is the cdf for the product of two independent Rician random variables with the same K factor.[2] When the cdfs of the Rician and the XYRician are computed, the amplitude of the specular component is set to one [15]. The XYRician distribution is considered because of the product form of the fading for modulated backscatter. The comparisons are made graphically and in terms of four different metrics that are based on the mean square error (MSE) between the measured and theoretical cdfs.

The deepest fades heavily influence the average probability of error over a fading channel [10]. To take this into consideration in curve fitting, the log of the cdf is considered in addition to the cdf. A second way we can emphasize the smaller cdf values is to calculate the MSE only for signal levels below the median [10], which is called "half scale" in this paper. The modified MSEs for the full and half scales are defined by

$$\mathrm{FMSE} = \frac{\sum_{x=-30}^{10} \left[\log_{10} F_n(x) - \log_{10} F(x)\right]^2}{N_{\mathrm{full}}} \quad (1)$$

$$\mathrm{HMSE} = \frac{\sum_{x=-30}^{0} \left[\log_{10} F_n(x) - \log_{10} F(x)\right]^2}{N_{\mathrm{half}}} \quad (2)$$

respectively. The values of the index x are envelope levels relative to the median, incremented in 1 dB steps. $F_n(x)$ is a measured cdf, and $F(x)$ is a theoretical cdf. N_{full} and N_{half}, which are 41 and 31, respectively, are the numbers of bins for the full and half scales, respectively. The MSEs computed on the linear scale are the same as in (1) and (2) except the logarithms are not taken. The various MSEs for each location are shown in Table I.

A couple of general comments about the table are helpful in its interpretation. First, the position of the boldfaced value indicates the particular metric that was used to optimize the parameter of the cdf. For example, for Location 1, 0.55 is the value of m that yields the best fit of the Nakagami distribution when the linear, full scale is used. Second, we observe that use of the

[1]There is 1 dB difference between this and the value in [14] since they were from different sets of data with different configurations.

[2]We use the approximation that two segments have the same Rician K factors.

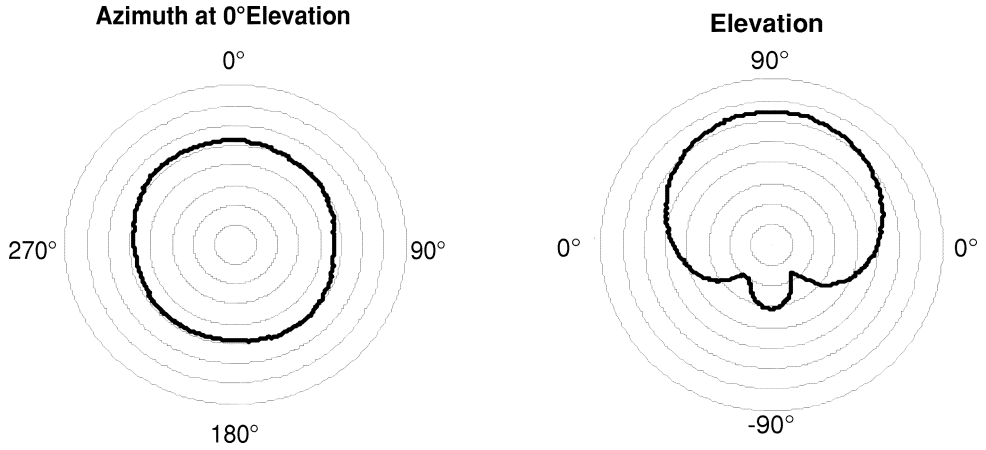

Fig. 5. Patch antenna patterns [7].

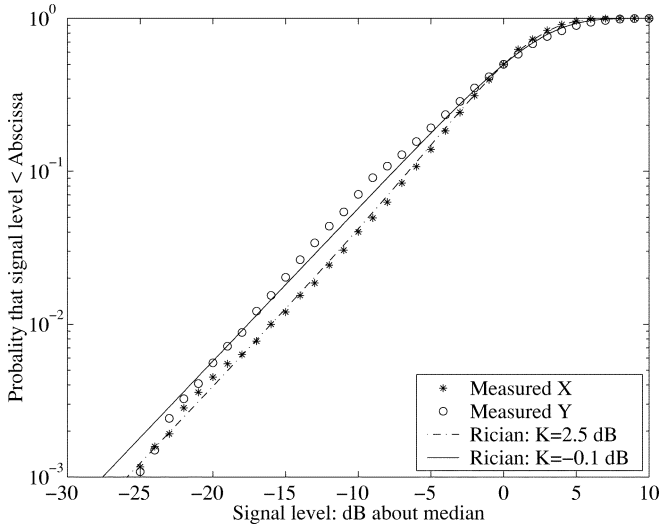

Fig. 6. One-way measurement with the EST antenna for Location 3. The solid and dashed lines are Rician cdfs for $K = -0.1$ dB and $K = 2.5$ dB, respectively.

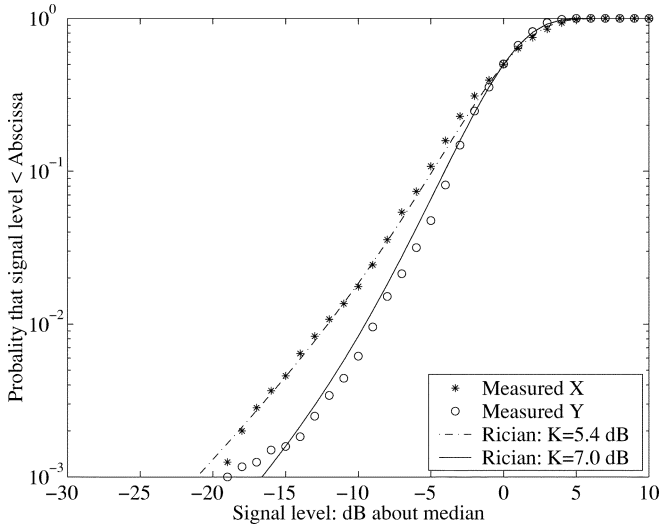

Fig. 7. One-way measurement with the patch antenna for Location 3. The solid and dashed lines are Rician cdfs for $K = 7.0$ dB and $K = 5.4$ dB, respectively.

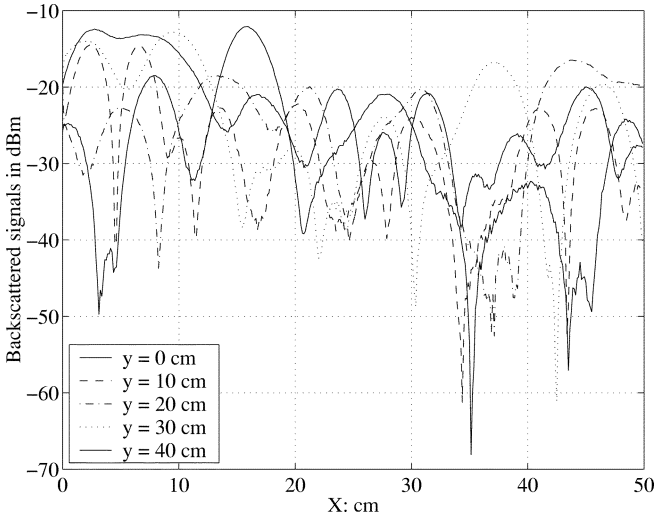

Fig. 8. Two-way faded envelopes of five scans for Location 1.

log scale weights the smaller values of the cdf so heavily that the choice of half or full scale becomes irrelevant. The XYRician with $K = -\infty$ dB is the same as the product of two independent Rayleigh distributions, and its cdf in a closed form can be derived using the integral tables in [16]. The cdf of the product-Rayleigh distribution is given by

$$F_Z(z) = 1 - \sqrt{\frac{z^2}{b_1 b_2}}\tilde{K}\left(\sqrt{\frac{z^2}{b_1 b_2}}\right) \tag{3}$$

where Z is the random variable representing the product of the fades on the two segments (i.e., $Z = XY$), b_1 and b_2 are the variances of the fades on each segment, respectively, and $\tilde{K}(\cdot)$ is the modified Bessel function of the second kind and the first order. The median value of Z is approximately $1.257\sqrt{b_1 b_2}$, which is found by numerical integration. When Z is normalized by its median value, (3) becomes independent of the variances like the single random variable Rayleigh distribution.

We observe that all values of m are less than one, indicating worse than Rayleigh fading [17], [18]. These low values are expected since occasionally both segments will be faded, producing an especially deep fade in the RFMB link.

TABLE I
FOUR MSE-BASED METRICS OF THE cdfs FOR THREE LOCATIONS

Location	CDF	Full scale			Half scale		
		Parameter	Log scale	Linear scale	Parameter	Log scale	Linear scale
1	XYRician; K	$-\infty$ dB	$\mathbf{4.92 \times 10^{-3}}$	7.90×10^{-5}	$-\infty$ dB	$\mathbf{6.50 \times 10^{-3}}$	7.23×10^{-5}
		$-\infty$ dB	4.92×10^{-3}	$\mathbf{7.90 \times 10^{-5}}$	$-\infty$ dB	6.50×10^{-3}	$\mathbf{7.23 \times 10^{-5}}$
	Nakagami; m	0.69	$\mathbf{2.82 \times 10^{-3}}$	1.02×10^{-3}	0.69	$\mathbf{3.42 \times 10^{-3}}$	2.23×10^{-4}
		0.55	3.76×10^{-2}	$\mathbf{3.50 \times 10^{-4}}$	0.61	1.77×10^{-2}	$\mathbf{4.34 \times 10^{-5}}$
	Log-normal; σ	10.8 dB	$\mathbf{6.14 \times 10^{-3}}$	2.28×10^{-3}	10.8 dB	$\mathbf{7.39 \times 10^{-3}}$	6.12×10^{-4}
		8.2 dB	3.08×10^{-1}	$\mathbf{5.74 \times 10^{-4}}$	9.2 dB	1.15×10^{-1}	$\mathbf{9.64 \times 10^{-5}}$
2	XYRician; K	$-\infty$ dB	$\mathbf{1.64 \times 10^{-3}}$	8.06×10^{-5}	$-\infty$ dB	$\mathbf{2.16 \times 10^{-3}}$	5.60×10^{-5}
		$-\infty$ dB	1.64×10^{-3}	$\mathbf{8.06 \times 10^{-5}}$	$-\infty$ dB	2.16×10^{-3}	$\mathbf{5.60 \times 10^{-5}}$
	Nakagami; m	0.71	$\mathbf{3.14 \times 10^{-3}}$	1.23×10^{-3}	0.71	$\mathbf{3.80 \times 10^{-3}}$	2.93×10^{-4}
		0.55	5.05×10^{-2}	$\mathbf{4.40 \times 10^{-4}}$	0.62	2.32×10^{-2}	$\mathbf{6.36 \times 10^{-5}}$
	Log-normal; σ	10.6 dB	$\mathbf{6.24 \times 10^{-3}}$	1.97×10^{-3}	10.6 dB	$\mathbf{7.60 \times 10^{-3}}$	5.13×10^{-4}
		8.2 dB	2.75×10^{-1}	$\mathbf{4.80 \times 10^{-4}}$	9.2 dB	9.34×10^{-2}	$\mathbf{6.54 \times 10^{-5}}$
3	XYRician; K	2.8 dB	$\mathbf{6.12 \times 10^{-4}}$	4.82×10^{-4}	2.8 dB	$\mathbf{6.58 \times 10^{-4}}$	3.75×10^{-5}
		0.5 dB	1.78×10^{-2}	$\mathbf{1.56 \times 10^{-4}}$	2.1 dB	4.52×10^{-3}	$\mathbf{6.76 \times 10^{-6}}$
	Nakagami; m	0.90	$\mathbf{9.66 \times 10^{-4}}$	9.62×10^{-4}	0.90	$\mathbf{9.75 \times 10^{-4}}$	8.10×10^{-5}
		0.72	5.77×10^{-2}	$\mathbf{4.90 \times 10^{-4}}$	0.82	1.49×10^{-2}	$\mathbf{1.72 \times 10^{-5}}$
	Log-normal; σ	9.2 dB	$\mathbf{2.23 \times 10^{-2}}$	2.48×10^{-3}	9.2 dB	$\mathbf{2.89 \times 10^{-2}}$	1.09×10^{-3}
		6.6 dB	9.35×10^{-1}	$\mathbf{2.23 \times 10^{-4}}$	7.2 dB	5.86×10^{-1}	$\mathbf{7.83 \times 10^{-5}}$

Of the three theoretical distributions considered, the XYRician has the best fit for nine of the 12 combinations of metrics and locations. The three exceptions are that Nakagami is preferred at Location 1: the log full-scale, the log half-scale, and the linear half-scale. In the nine combinations for which the XYRician is the best fit, the Nakagami and the log-normal have eight and one combinations, respectively, for the next best fit. The optimal K factor for the XYRician varies between $-\infty$ dB and 2.8 dB for all combinations of metrics and locations. The low values of K for these LOS configurations may be explained by strong reflections from nearby metal cabinets and bookshelves.

The results in Table I are quite similar to the table in [14], where the XYRician has the best fit for 10 of the 12 combinations. This minor difference results from the orientation of the EST. For this paper, the EST was oriented sideways relative to the T-shaped fixture, as shown in Fig. 4 whereas it was mounted flat on the top of the fixture in [14]. The sideways orientation is more like the flush position of the antenna when it is deployed as a shelf tag.

Figs. 9 and 10 show the measured cdfs for the sample sets of Locations 1 and 2, respectively, along with the best fitting theoretical cdfs (in terms of MSE of the logs of the cdfs). All cdfs are normalized to the median level for convenient comparison. The Rayleigh and Rician with $K = 6$ dB distributions are also shown in the figures as a reference.

Consistent with our earlier observations about m, the measured cdfs show that two-way fading is more severe than traditional one-way fading. For example, in Fig. 9, the two-way

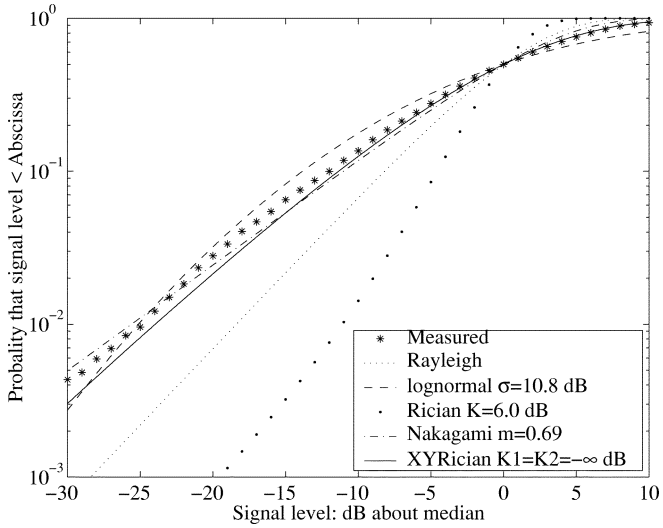

Fig. 9. Measured cdf for Location 1.

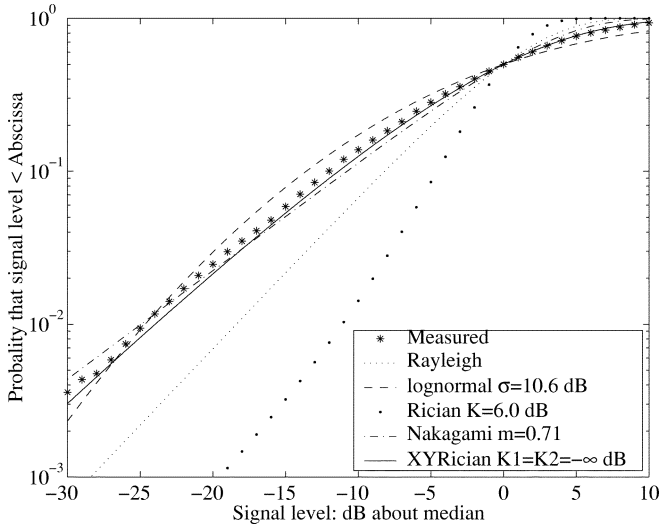

Fig. 10. Measured cdf for Location 2.

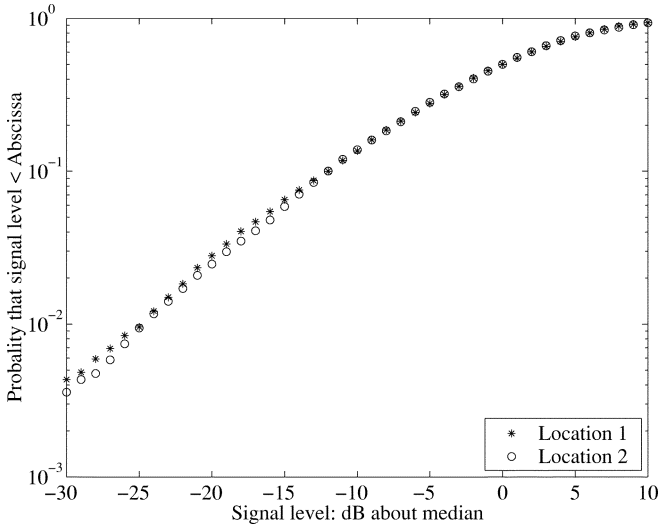

Fig. 11. Measured cdfs for Locations 1 and 2.

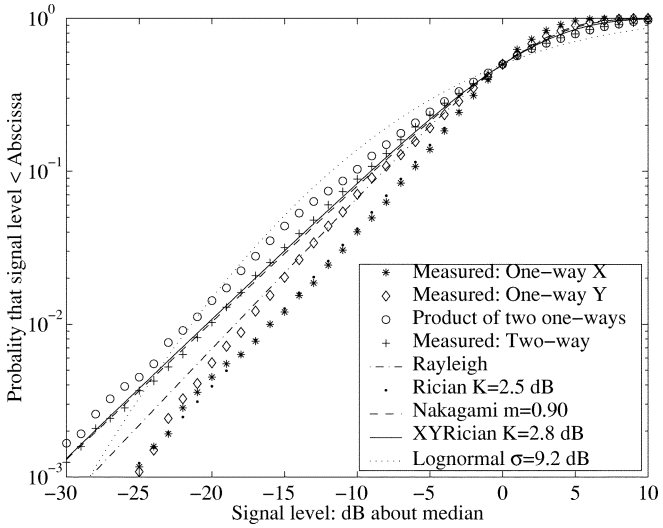

Fig. 12. The measured cdfs for Location 3.

fade at the 1% level (i.e., at probability $= 10^{-2}$) is approximately 7 dB lower than the fade at the 1% level for the Rayleigh distribution. This means that the fade margin for a modulated backscatter link to ensure 99% availability would be 7 dB larger than the fade margin for a one-way Rayleigh-faded link with the same median path loss.

Fig. 11 compares the measured cdfs for Locations 1 and 2. The middle parts of the measured cdfs are very similar, but the tail parts are slightly different. The different cluttering environment between Locations 1 and 2 may explain this cdf discrepancy. Location 2 is relatively clutter-free compared to Location 1. In Location 1, there are metal bookshelves alongside the actuator setup. The MSEs between these curves are 1.24×10^{-3} and 1.64×10^{-3} for the full and half scales, respectively. These low MSE values indicate cdf repeatability with the same geometry in the same room.

To further investigate the product-based model of the fading, we considered the distributions and correlation of the fades for the individual segments. The correlation coefficient ρ_{XY} of the one-way fades was found as follows. Let X and Y be $N \times 1$ column vectors of fade samples such that their ith elements, x_i and y_i, are the measured envelopes at the carrier frequency for the first and second segments, respectively, when the tag is in the ith position. Then

$$\rho_{XY} = \frac{\frac{X^T Y}{N} - \bar{X}\bar{Y}}{\sqrt{\bar{\sigma}_X^2 \bar{\sigma}_Y^2}} \tag{4}$$

where $\bar{X}$ and $\bar{Y}$ are sample means and $\bar{\sigma}_X^2$ and $\bar{\sigma}_Y^2$ are sample variances. For $N = 12\,000$ samples, $\rho_{XY} = 0.046$, indicating almost no correlation between the fades of the two segments.

Next, we identified the best-fitting distributions to the fades of the individual segments. The cdfs are shown in Fig. 12. The cdf of each segment is close to the Rayleigh distribution in spite of the presence of LOS on both branches of propagation. This may be explained by the lack of directionality of the EST antenna.

Finally, for each tag location, we multiplied the individual segment fades and found the cdf of the resulting collection of products to get the curve indicated by circles in Fig. 12. This curve is fairly close to the cdf of the measured two-way fades.

Specifically, the MSEs between the two curves are within 8.08×10^{-3} in terms of FMSE, and within 1.07×10^{-2} in terms of HMSE. The small differences may be explained by the fact that one of the ceiling antennas was exchanged with another similar one for the one-way measurement and the other ceiling antenna may have been moved slightly when connections were changed.

IV. Analysis of Median Path Loss

The wireless channel for modulated backscatter consists of two segments: the unmodulated and the modulated segments. Hence, the relationship between transmitted power P_t and received power P_r should include the contributions of the two segments and the EST. In free space, the relationship can be expressed as [2], [3]

$$\frac{P_r}{P_t}=\underbrace{\left[G_tg_r\left(\frac{\lambda}{4\pi d_1}\right)^2\right]}_{\text{Segment 1}}\underbrace{[\Gamma\Omega]}_{\text{EST}}\underbrace{\left[G_rg_t\left(\frac{\lambda}{4\pi d_2}\right)^2\right]}_{\text{Segment 2}} \tag{5}$$

and this can be rearranged to

$$\frac{P_r}{P_t}=G_tG_r(g_t\Gamma g_r)\Omega\left(\frac{\lambda}{4\pi}\right)^4\left(\frac{1}{d_1d_2}\right)^2 \tag{6}$$

where G_t and G_r are the gains of Antennas 1 and 2, respectively, in the direction of the tag. g_t and g_r are the EST's antenna gains toward Antennas 1 and 2, respectively, both considered to be 0 dBi. The wavelength, λ, is 12.5 cm at 2.4 GHz, d_1 and d_2 are the lengths of the unmodulated and the modulated segments, respectively, Γ is the reflection coefficient of the EST antenna, and Ω is the modulation loss due to detecting the first harmonic [2].

For a generalized path loss model for symmetric geometries, the path loss L_p in decibels is given by

$$L_p=L_0+10n\log d_1+10n\log d_2 \tag{7}$$

where $L_0=10\log P_t-10\log P_0$ and P_0 are the path loss and the normalized received power, respectively, at a distance of 2 m$(d_1=d_2=1$ m$)$ and where n is a path loss exponent.

Eqn. (7) can be extended to asymmetric geometries, $d_1\neq d_2$. Defining $D=\sqrt{d_1d_2}$, (7) reduces to

$$L_p=L_0+10N\log D \tag{8}$$

where $N=2n$ is a path loss exponent in the two-way link, which is 4 in free space.

Since the distances of the two-way link are a function of two ceiling antenna locations, the path loss measurements were carried out on contours that have same geometric means. This was done for three different ceiling antenna separations. Figs. 13–15 show the D-contours and local median values of the path loss for antenna separations of 4 m, 7 m, and 11 m, respectively.

In these figures, each "*" represents a local area, and the corresponding median value of its fades is indicated beside it. Using the Wilcoxon formula in [12], these median values are in the 95% confidence interval. Because of the large table in the conference room, the path loss measurements could not be taken on contours for $D<4$ m.

The path loss measurements in the conference room are shown in Fig. 16. Linear regression [19] is used for estimating

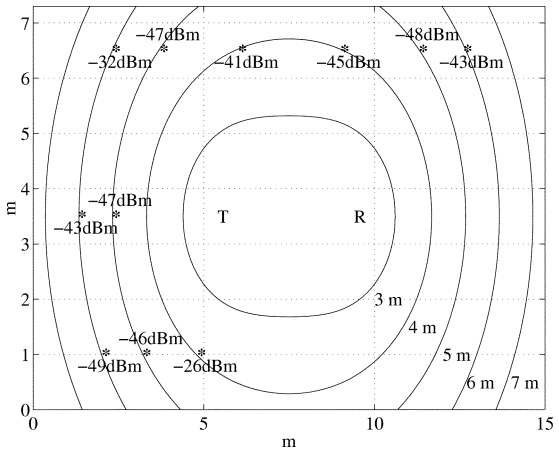

Fig. 13. Contours and local median values for antenna separation of 4 m in the conference room.

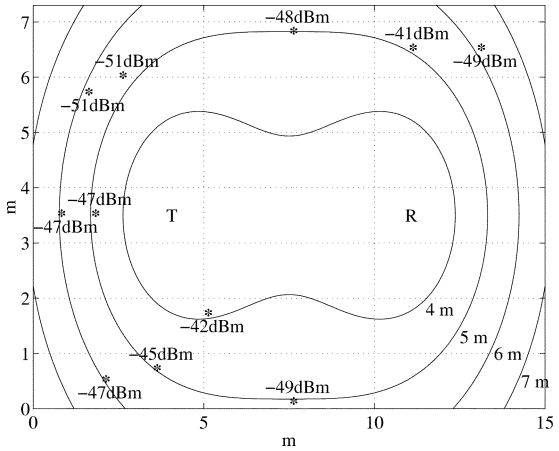

Fig. 14. Contours and local median values for antenna separation of 7 m in the conference room.

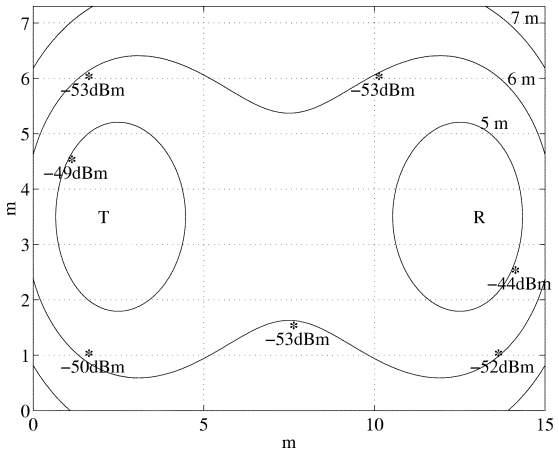

Fig. 15. Contours and local median values for antenna separation of 11 m in the conference room.

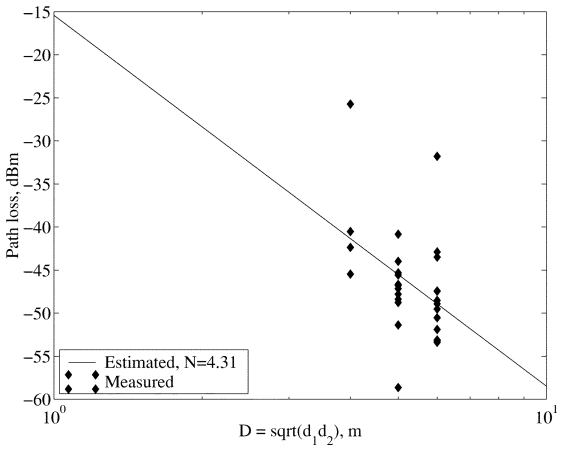

Fig. 16. Path loss for the two-way link in the conference room.

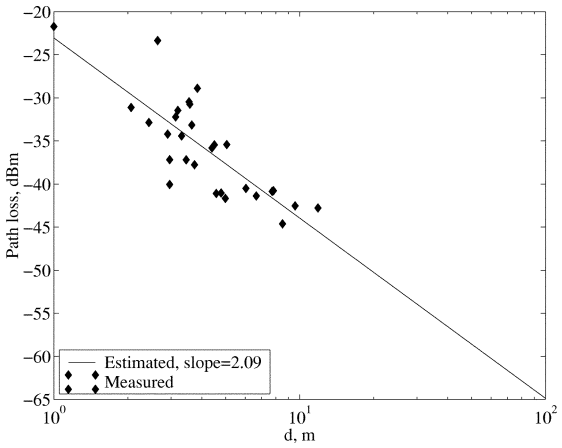

Fig. 17. Path loss for the one-way link in the conference room.

a path loss exponent. The path loss exponent is about 4.31 with the standard deviation of 6.7 dB. For comparison, path loss measurements for the one-way link were also carried out on the same contours shown in Figs. 13, 14, and 15. The path loss of the one-way link is shown in Fig. 17. The path loss exponent of the one-way link is 2.09 with the standard deviation of 7.6 dB. The reported path loss exponents of one-way links in lightly cluttered environments range from 1.4 to 3.4 [15], [20]. Since the conference room is a very lightly cluttered environment, the expected path loss exponent is about 2, and the measured path loss exponent is close to the expected.

The discrepancy of the path loss exponents between the two-way link and two-fold of the one-way link is 0.13, which results in 1.3 dB difference at every decade of distance. This discrepancy might be explained by slight differences of the locations of the ceiling antennas and the EST as well as minor environment changes. It might also be explained by variations in the statistics.

V. Conclusion

Small-scale fading statistics and median path loss measurements for the CW-type of RFMB in an indoor, small office environment at 2.4 GHz have been presented. The small-scale fading statistics show significantly deep fades in spite of the presence of LOS on both segments of propagation. The fading results suggest that the small-scale fading on a modulated backscatter link can be modeled by a product of independent Rician random variables, by a log-normal random variable, or by a Nakagami random variable, with product Rician being the best in terms of MSE of the cdf.

The path loss measurements confirm that the path loss exponent of the two-way link is approximately twice that of a traditional one-way link in the same environment. This suggests link budgets for the modulated backscatter channels can use the many published propagation results for one-way links.

Acknowledgment

The authors would like to thank Dr. A. Claessen of NCR for his helpful suggestions in the course of this work, and the reviewers for their thoughtful comments.

References

[1] P. T. Blythe, "RFID for road tolling, road-use pricing and vehicle access control," in *Inst. Elec. Eng. Colloquium on RFID Technol.*, London, U.K., Oct. 1999, pp. 8/1–8/16.

[2] J. G. Evans, R. A. Shober, S. A. Wilkus, and G. A. Wright, "A low-cost radio for an electronic price label system," *Bell Labs Tech. J.*, pp. 203–215, Autumn 1996.

[3] K. Finkenzeller, *RFID Handbook: Radio-Frequency Identification Fundamentals and Applications*. West Sussex, U.K.: Wiley, 1999.

[4] J. R. Tuttle, "Traditional and emerging technologies and applications in the radio frequency identification (RFID) industry," in *Proc. IEEE Radio Freq. Integrated Circuits Symp.*, Denver, CO, June 1997, pp. 5–8.

[5] K. V. S. Rao, "An overview of back scattered radio frequency identification system (RFID)," in *Proc. IEEE Asia Pacific Microwave Conf.*, vol. 3, Singapore, Dec. 1999, pp. 746–749.

[6] G. W. Stimson, *Introduction to Airborne Radar*. El Segundo, CA: Hughes Aircraft Company, 1983.

[7] 2.4 GHz Patch Antenna for ISM Band, M/A-COM. (2002, Feb.). *http://www.macom.com/data/datasheet/1307031.pdf* [Online]

[8] M. Kossel, H. R. Benedickter, R. Peter, and W. Bächtold, "Microwave backscatter modulation systems," in *Proc. IEEE MTT-S Int. Microwave Symp.*, vol. 3, Boston, MA, June 2000, pp. 1427–1430.

[9] H. Hashemi, "The indoor radio propagation channel," *Proc. IEEE*, vol. 81, pp. 943–967, July 1993.

[10] K. Pahlavan and A. H. Levesque, *Wireless Information Networks*. Chichester: Wiley, 1995.

[11] W. C. Jakes, *Microwave Mobile Communications*. New York: IEEE Press, 1993.

[12] D. Zwillinger, *Standard Mathematical Tables and Formulae*, 30th ed. Boca Raton: CRC Press, 1996.

[13] H. Hashemi, M. McGuire, T. Vlasschaert, and D. Tholl, "Measurements and modeling of temporal variations of the indoor radio propagation channel," *IEEE Trans. Veh. Technol.*, vol. 43, no. 3, pp. 733–737, Aug. 1994.

[14] D. Kim, M. A. Ingram, and W. W. Smith Jr., "Small-scale fading for an indoor wireless channel with modulated backscatter," in *Proc. IEEE Veh. Technol. Conf.*, vol. 3, Atlantic City, NJ, Oct. 2001, pp. 1616–1620.

[15] T. S. Rappaport and C. D. McGillem, "UHF fading in factories," *IEEE J. Select. Areas Commun.*, vol. 7, no. 1, pp. 40–48, Jan. 1989.

[16] I. S. Gradshteyn and I. M. Ryzhik, *Table of Integrals, Series, and Products*, 5th ed. San Diego: Academic, 1994.

[17] J. G. Proakis, *Digital Communications*, 3rd ed. New York: McGraw-Hill, 1995.

[18] G. L. Stüber, *Principles of Mobile Communication*, 2nd ed. Boston, MA: Kluwer, 2001.

[19] W. J. Dixon and F. J. Massey Jr., *Introduction to Statistical Analysis*, 4th ed. New York: McGraw-Hill, 1983.

[20] D. Molkdar, "Review on radio propagation into and within buildings," *Inst. Elec. Eng. Proc.-H*, vol. 138, no. 1, pp. 61–73, Feb. 1991.

Daeyoung Kim (S'89–M'02) received the Bachelor and Master degrees in electronic engineering from Hanyang University, Seoul, Korea, in 1989 and 1991, respectively, and the Ph.D. degree in electrical engineering from the Georgia Institute of Technology, Atlanta, in 2002.

From 1991 to 1998, he was a Research Engineer with the Samsung Electronics Company Ltd., Yongin, Korea, where he was involved in the DSP F/W development and applications of a fax modem IC and the implementation of error correction codes. He is currently with Samsung Electronics Company Ltd., Suwon, Korea. His research interests are wireless channel propagation measurements and modeling, RFID systems, array signal processing, and communication systems.

Mary Ann Ingram (S'84–M'89) received the B.E.E. and Ph.D. degrees from the Georgia Institute of Technology (Georgia Tech), Atlanta, in 1983 and 1989, respectively.

From 1983 to 1986, she was a Research Engineer with the Georgia Tech Research Institute, Atlanta, performing studies on radar electronic countermeasure (ECM) systems. In 1986, she became a graduate research assistant with the School of Electrical and Computer Engineering at Georgia Tech. After graduating, she became a faculty member at Georgia Tech, where she is currently an Associate Professor. Her early research areas were optical communications and radar systems. Since 1997, she has focused on the application of multiple-antenna systems to wireless communications.

W. Whit Smith, Jr. (M'00) received the Bachelor, Master, and Ph.D. (1990) degrees in electrical engineeering from the Georgia Institute of Technology, Atlanta, with intervening industry experience including the development of broadcast transmitters and industrial controls.

He is a Senior Research Engineer within Georgia Tech's School of Electrical and Computer Engineering. His interests include satellite communications, mixed analog and digital instrumentation, and student development. In addition to performing teaching and industry sponsored research, between 1992 and 1997, he presided over about 150 students who refurbished a former AT&T satellite earth station, consisting of a pair of 100 foot dish antennas, to create a satellite and radio astronomy facility. He also consults as a licensed Professional Engineer. Although, he had not planned to teach, he hosted and continues to sponsor a variety of undergraduate and K-12 student-oriented research projects.

Dr. Smith received the 2000 Electrical and Computer Engineering School's Outstanding Teacher Award.